Interplay between charge and spin thermal entanglement in Hubbard dimers

Fabiana Souza, Guilherme M. A. Almeida, Marcelo L. Lyra, and Maria S. S. Pereira
Instituto de Física, Universidade Federal de Alagoas, 57072-970 Maceió-AL, Brazil

We study quantum entanglement in half-filled Hubbard dimers at finite temperatures under an external magnetic field. Due to the itinerant nature of the electrons and their fundamental indistinguishability, we employ a site-based evaluation of entanglement via the concurrence in three distinct sectors of the Hilbert space, namely the charge, zero-, and single-spin subspaces. At zero temperature these measures can be combined to produce an accurate estimate of the entanglement entropy. For finite temperatures we show that those concurrences display reentrant behavior upon varying the magnetic field. Furthermore, we unveil that charge and spin quantum correlations are quite distinctly degraded by thermal fluctuations.

I. INTRODUCTION

Quantum entanglement, a peculiar trait of composite quantum systems, is a key resource in many quantum information processing protocols, such as quantum key distribution and teleportation, and also plays a significant role in the behavior of many-body systems, which is tightly connected to quantum phase transitions [1–3]. Its proper characterization has thus been the subject of intensive research activity. Basically, entanglement quantifiers must be able to assess the degree of quantum correlations available in nonseparable multiparty quantum systems and return a number, which is not straightforward in general [4]. The entanglement properties of bipartite pure states with distinguishable parties (say, two qubits) are, on the other hand, fairly well understood via the Schmidt decomposition of the state or, alternatively, via calculation of the von Neumann entropy of either of the reduced density matrices. (It is worth pointing out that the usefulness of the spectral properties of the reduced statistical operators goes way beyond entropic measures to provide relevant information regarding the underlying entanglement Hamiltonian [5–8].)

Subsystems of a many-body pure state are mixed states in general. In this situation, it is a challenging task to find a practical quantifier able to discriminate genuine bipartite entanglement from correlations shared with the external degrees of freedom. This is of paramount importance, for instance, when dealing with systems in equilibrium with a thermal bath, where the so-called thermal entanglement sets about [2,9,10]. For the evaluation of the pairwise entanglement of mixed states, a frequently used measure is the entanglement of formation [11] which, given a density matrix operator ρ, calls for the amount of pure-state entanglement necessary to form it and takes the minimum over all pure-state decompositions of ρ (a null outcome means that ρ can be created locally without any entangled pure states). The downside is that there are infinitely many decompositions of ρ, turning the evaluation of the entanglement of formation into a very difficult problem. For two qubits, fortunately, there exists an analytic solution, often expressed in terms of a quantity called concurrence [12,13], which is monotonically related to the former. It is thus not surprising that concurrence became a powerful tool to quantify entanglement in a wide range of contexts. Despite being very practical to handle, concurrence, as originally conceived [12,13], is suited for quantum states having each partition featuring a bidimensional Hilbert space, such as spatially separated (meaning distinguishable) spin-1/2 particles. In fact, our standard knowledge of entanglement is well established only in the case of distinguishable particles, which underlies the majority of quantum information processing schemes. This scenario is nicely justified when then the single-particle wave functions of the quantum registers barely overlap with each other. If they do, then the exchange symmetry comes into play, for identical particles are fundamentally indistinguishable.

The entanglement of identical particles is a very subtle concept. The issue manifests already from the lack of a simple tensor product structure for the composite system as (fermions) bosons must obey the (anti)symmetrization postulate. As a consequence, states accounting for identical particles display intrinsic correlations by construction, and thus long-standing topics of debate are whether or not those states are entangled (cf. Refs. [14,15] for pertinent advances on that matter), how to partition them, and how to quantify it [14–39]. The search for entanglement measures for systems of identical particles is also timely for the proper characterization of several classes of condensed matter models. In particular, much attention has been given to quantum entanglement in strongly correlated lattice systems with itinerant electrons [21,22,27,40–45]. In doing so, a convenient approach is to quantify entanglement between the modes [21–23,25,31–33,35–37] rather than between the particles as many-body models rely on the second-quantization language, and it is desirable to deal with subsystems which can be operationally distinguished (that is, easily accessible by measurements). In the case of delocalized electrons in a lattice, the partitions may be chosen to be sites [23].

TABLE I. Eigenenergies and eigenvectors of the Hubbard-dimer Hamiltonian. $\Delta = U^2 + 16t^2$; $\alpha_1 = (U - \sqrt{\Delta})/4t$; $\alpha_2 = (U + \sqrt{\Delta})/4t$; $a = 2t/\sqrt{\Delta - U\sqrt{\Delta}}$; $b = 2t/\sqrt{\Delta + U\sqrt{\Delta}}$. $|\lambda_2\rangle$ and $|\lambda_5\rangle$ are the two possible ground states.

Eigenenergy	Eigenvector
$\lambda_1 = \frac{U+\sqrt{\Delta}}{2}$	$\|\lambda_1\rangle = a(\| \uparrow\downarrow\rangle \otimes \|0\rangle + \|0\rangle \otimes \| \uparrow\downarrow\rangle - \alpha_1 \| \uparrow\rangle \otimes \| \downarrow\rangle - \alpha_1 \| \downarrow\rangle \otimes \| \uparrow\rangle)$
$\lambda_2 = \frac{U-\sqrt{\Delta}}{2}$	$\|\lambda_2\rangle = b(\| \uparrow\downarrow\rangle \otimes \|0\rangle + \|0\rangle \otimes \| \uparrow\downarrow\rangle - \alpha_2 \| \uparrow\rangle \otimes \| \downarrow\rangle - \alpha_2 \| \downarrow\rangle \otimes \| \uparrow\rangle)$
$\lambda_3 = U$	$\|\lambda_3\rangle = \frac{1}{\sqrt{2}}(\| \uparrow\downarrow\rangle \otimes \|0\rangle - \|0\rangle \otimes \| \uparrow\downarrow\rangle)$
$\lambda_4 = 0$	$\|\lambda_4\rangle = \frac{1}{\sqrt{2}}(\| \uparrow\rangle \otimes \| \downarrow\rangle - \| \downarrow\rangle \otimes \| \uparrow\rangle)$
$\lambda_5 = -2H$	$\|\lambda_5\rangle = \| \uparrow\rangle \otimes \| \uparrow\rangle$
$\lambda_6 = 2H$	$\|\lambda_6\rangle = \| \downarrow\rangle \otimes \| \downarrow\rangle$

The entanglement-of-modes approach, as put forward by Zanardi [21], is based on the mapping of the Fock space into a state space of qubits. Following that, we can then proceed with standard measures of entanglement, such as concurrence [12]. However, even in the simplest case of lattice sites having a single orbital supporting at most two electrons (with opposite spins), the local Hilbert space is four dimensional, thus apparently ruling out the use of concurrence measures. Despite that, concurrence has been explored in judiciously restricted Hilbert subspaces, thereby giving partial information regarding to underlying quantum entanglement [46–52]. For instance, single-site entanglement has been addressed in Ref. [46] and partial fermionic concurrences defined for specific degrees of freedom (charge and spin) have been studied in Ref. [51]. Here, we build on the latter and contribute to the characterization of quantum entanglement in strongly correlated electron systems by introducing a full set of concurrence measures for two-site entanglement. As a prototype model, we consider a Hubbard dimer in thermal equilibrium with a heat bath and under the action of an external magnetic field. We show that partial concurrences, defined through proper mappings of the local modes of the system into effective qubits in three distinct sets, namely polarized charge, zero-, and single-spin subspaces, provide a rich description of the entanglement. Further, we find out that those three contributions display quite distinct sensitivities to thermal fluctuations. We consider a Hubbard dimer only for the sake of simplicity. The whole method described in this paper is easily extended to N-site Hubbard lattices.

II. HUBBARD-DIMER: EIGENSTATES AND VON NEUMANN ENTROPIES

We consider a half-filled Hubbard dimer under a finite magnetic field as a prototype model to study site entanglement in a system of itinerant electrons. Let us start by reviewing some basic aspects related to the model Hamiltonian and its spectral properties. Considering $c_{i,\gamma}^\dagger$ and $c_{i,\gamma}$ the fermionic creation and annihilation operators for an electron with spin $\gamma = \uparrow, \downarrow$ at site $i = 1, 2$, with $n_{i,\gamma} = c_{i,\gamma}^\dagger c_{i,\gamma}$ being the respective number operator, and S_i^z accounting for the z component of the total spin operator at site i, the Hubbard Hamiltonian reads

$$\mathcal{H} = t \sum_{\gamma=\uparrow,\downarrow} (c_{1,\gamma}^\dagger c_{2,\gamma} + \text{H.c.}) + \sum_{i=1}^{2} (U n_{i,\uparrow} n_{i,\downarrow} - H S_i^z), \quad (1)$$

where t is the hopping amplitude associated with the mobility of electrons between the lattice sites. Note that this process is restricted to electrons in distinct spin states due to the Pauli's exclusion principle. H is an external magnetic field and U is the on-site Hubbard interaction, which can be taken to assume positive (negative) values accounting for an effective repulsive (attractive) electron-electron interaction. In the half-filled configuration with just two electrons, the Hilbert space is spanned by six possible configurations, $\{|\uparrow\downarrow; 0\rangle, |0; \uparrow\downarrow\rangle, |\uparrow; \downarrow\rangle, |\downarrow; \uparrow\rangle, |\uparrow; \uparrow\rangle, |\downarrow; \downarrow\rangle\}$, where, e.g., $|\uparrow\downarrow; 0\rangle$ is short for $|\uparrow\downarrow\rangle \otimes |0\rangle$. The stationary Hamiltonian eigenstates $|\lambda_i\rangle$ and their respective eigenenergies λ_i are listed in Table I. There are two-possible ground states. For large magnetic fields, the fully polarized separable $|\lambda_5\rangle$ gets the minimal energy. On the other hand, the nonseparable state $|\lambda_2\rangle$ becomes the ground state at low fields. For finite magnetic fields, there is a critical Hubbard coupling U^* separating these two ground states given by $U^*/t = 2(t/H - H/t)$. The ground-state phase diagram is illustrated in Fig. 1.

Out of the six Hamiltonian eigenstates, the first four with electrons in distinct spin states are nonseparable. To quantify the degree of quantum entanglement in these pure states, one can simple evaluate the von Neumann entropy of entanglement for state $|\lambda_i\rangle$ given by $\mathcal{S}_i = -\text{Tr}\, \rho_1 \ln \rho_1$, where ρ_1 is
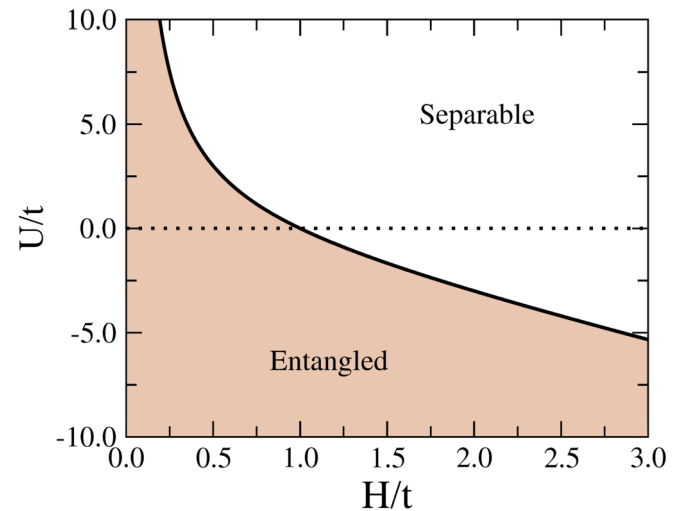
FIG. 1. Ground-state phase diagram for the half-filled Hubbard dimer in U/t vs H/t parameter space. The fully polarized state that overcomes at large magnetic fields is separable while the quantum entangled state $|\lambda_2\rangle$ predominates at low fields.

TABLE II. Expectation values of the dimer correlations associated with the density matrix elements of Eq. (3) in each two-qubit sector, namely charge ($X = C$), single-spin ($X = 1$), and zero-spin ($X = 0$) sectors. Note that the resulting density matrices for sectors $X = 1$ and $X = 0$ are not normalized since both consist of parts (projections) of the full one with 16×16 entries, unlike the one corresponding to $X = C$, which is normalized as the projection operators (diagonal entries) form a complete space on their own. This and other details over the derivation of those matrices can be found in the Appendix.

ρ^X element	$X = C$	$X = 1$	$X = 0$
u_+	$\langle(1 - n_{1\uparrow})(1 - n_{2\uparrow})\rangle$	$\langle n_{1\uparrow}(1 - n_{1\downarrow})n_{2\uparrow}(1 - n_{2\downarrow})\rangle$	$\langle(1 - n_{1\uparrow})(1 - n_{2\uparrow})(1 - n_{1\downarrow})(1 - n_{2\downarrow})\rangle$
u_-	$\langle n_{1\uparrow}n_{2\uparrow}\rangle$	$\langle(1 - n_{1\uparrow})n_{1\downarrow}(1 - n_{2\uparrow})n_{2\downarrow}\rangle$	$\langle(n_{1\uparrow}n_{1\downarrow})(n_{2\uparrow}n_{2\downarrow})\rangle$
z	$\langle c_{1\uparrow}^\dagger c_{2\uparrow}\rangle$	$\langle c_{2\uparrow}^\dagger c_{2\downarrow}c_{1\downarrow}^\dagger c_{1\uparrow}\rangle$	$\langle c_{1\uparrow}^\dagger c_{1\downarrow}^\dagger c_{2\downarrow}c_{2\uparrow}\rangle$
x	$\langle n_{1\uparrow}(1 - n_{2\uparrow})\rangle$	$\langle n_{1\uparrow}(1 - n_{1\downarrow})(1 - n_{2\uparrow})n_{2\downarrow}\rangle$	$\langle(1 - n_{1\uparrow})(1 - n_{1\downarrow})(n_{2\uparrow}n_{2\downarrow})\rangle$
y	$\langle(1 - n_{1\uparrow})n_{2\uparrow}\rangle$	$\langle(1 - n_{1\uparrow})n_{1\downarrow}n_{2\uparrow}(1 - n_{2\downarrow})\rangle$	$\langle(n_{1\uparrow}n_{1\downarrow})(1 - n_{2\uparrow})(1 - n_{2\downarrow})\rangle$

the partial density matrix obtained after performing the partial trace of $\rho = |\lambda_i\rangle\langle\lambda_i|$ over the degrees of freedom associated with the dimer site 2. Both states $|\lambda_3\rangle$ and $|\lambda_4\rangle$ have entanglement entropy $\mathcal{S}_3 = \mathcal{S}_4 = \ln 2$ as they are of the Bell type. In contrast, the degree of entanglement in states $|\lambda_1\rangle$ and $|\lambda_2\rangle$ depends on the ratio U/t. Direct algebra provides

$$\mathcal{S}_1 = \mathcal{S}_2 = -2a^2\big[\ln(a^2) + \alpha_1^2 \ln\big(a^2\alpha_1^2\big)\big], \qquad (2)$$

where the coefficients a and α_1 are given in the caption of Table I. For noninteracting electrons ($U = 0$) one has $\mathcal{S}_1 = \mathcal{S}_2 = \ln 4$, because, after the partial trace, each site features an even mixing among its four possible configurations. The entanglement entropy of these states continuously decreases as stronger electron-electron couplings set in, converging to $\mathcal{S}_1 = \mathcal{S}_2 = \ln 2$ for infinite Hubbard coupling. In this limit, Bell-type forms are recovered.

III. CHARGE AND SPIN QUANTUM ENTANGLEMENT MEASURES

The above entanglement picture based on the von Neumann entropy does not allow for the identification of which degrees of freedom of the interacting electrons are actually quantum correlated. Along this direction, one can quantify the degree of entanglement in specific sectors of the Hilbert space [46–52]. The charge degrees of freedom are associated to each site allowing for basis vectors $|0\rangle$ and $|\uparrow\rangle$ within each dimer site. In this sector, the resulting reduced Hilbert space is $\{|0; 0\rangle, |0; \uparrow\rangle, |\uparrow; 0\rangle, |\uparrow; \uparrow\rangle\}$. The entanglement between the spin degrees of freedom can be evaluated in two other distinct sectors. Allowing for $|0\rangle$ and $|\uparrow\downarrow\rangle$ locally, we build the zero-spin sector spanned by $\{|0; 0\rangle, |0; \uparrow\downarrow\rangle, |\uparrow\downarrow; 0\rangle, |\uparrow\downarrow; \uparrow\downarrow\rangle\}$. The last sector involves a single spin in each site, $|\uparrow\rangle$ and $|\downarrow\rangle$, resulting in $\{|\uparrow; \uparrow\rangle, |\uparrow; \downarrow\rangle, |\downarrow; \uparrow\rangle, |\downarrow; \downarrow\rangle\}$ overall. In all those sectors, the dimer effectively behaves as two distinguishable qubits for which the quantum concurrence can be used as an accurate measure of entanglement. The density matrix in any of these three sectors can be put in the general form

$$\rho^X = \begin{pmatrix} u_+^X & 0 & 0 & 0 \\ 0 & x^X & z^X & 0 \\ 0 & (z^X)^* & y^X & 0 \\ 0 & 0 & 0 & u_-^X \end{pmatrix},$$

where $X = C, 0, 1$ stands for charge, zero-spin, and single-spin sectors, respectively, and the elements are given in terms of expectations values of distinct correlations between the dimer sites. These are given in Table II for each one of the above sectors (see the Appendix for details).

From the density matrix in these two-qubit sectors, one can readily compute the quantum concurrence in each subspace following the standard prescription found in Refs. [12,13]. The resulting expression for the partial concurrence reads

$$\mathcal{C}_X = 2 \max\{0, |z^X| - \sqrt{u_+^X u_-^X}\}, \qquad (3)$$

The outcomes for each one of the four entangled eigenstates are summarized in Table III so as to provide a general picture of how entanglement is weighted over those sectors. Note that for eigenstate $|\lambda_3\rangle$ the entanglement is fully manifested as quantum correlations in the zero-spin sector. Its Bell-type shape results in maximal two-qubit entanglement with $\mathcal{C}_0 = 1$ and $\mathcal{S} = \ln 2$, whereas there are no correlations in the charge and single-spin subspaces, in contrast with $|\lambda_4\rangle$, for which entanglement is restricted to a single-spin sector.

Entanglement is distributed in all three sectors for $|\lambda_1\rangle$ and $|\lambda_2\rangle$ eigenstates. Both have identical quantum correlations in the charge sector but distinct correlations in the zero- and single-spin counterparts. The dependence of these partial concurrences on the Hubbard coupling is shown in Fig. 2 for eigenstate $|\lambda_2\rangle$, in comparison with its entanglement entropy. Notice that in the strongly repulsive limit ($U \to \infty$) the contribution to entanglement comes solely from the single-spin sector, which is maximum as accounted for by the partial concurrence. In the opposite limit of a strongly attractive electron-electron interaction, entanglement results exclusively from correlations taking place in the zero-spin sector. Charge

TABLE III. Charge, single-, and zero-spin concurrences for each one of the entangled eigenstates of the Hubbard dimer. Terms a, b, α_1, and α_2 are available in the caption of Table I.

$|\lambda_i\rangle$	C_c	C_1	C_0
$|\lambda_1\rangle$	$4a^2\alpha_1$	$2a^2\alpha_1^2$	$2a^2$
$|\lambda_2\rangle$	$4b^2\alpha_2$	$2b^2\alpha_2^2$	$2b^2$
$|\lambda_3\rangle$	0	0	1
$|\lambda_4\rangle$	0	1	0
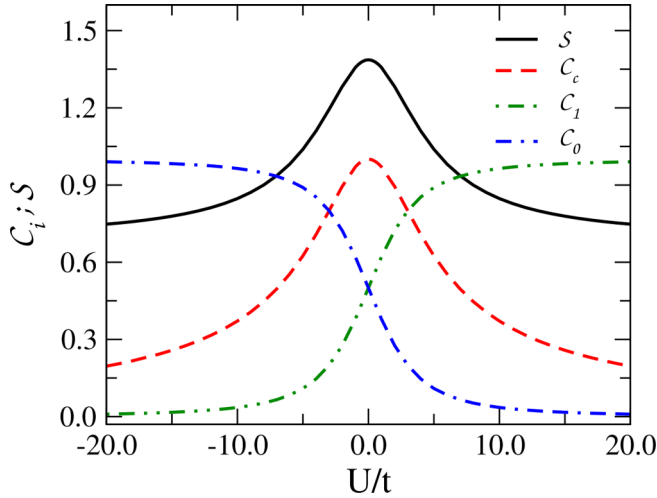
FIG. 2. Charge $\mathcal{C}_c$, single-spin $\mathcal{C}_1$, and zero-spin $\mathcal{C}_0$ concurrences as a function of the Hubbard coupling U/t for $|\lambda_2\rangle$ alongside its entanglement entropy $\mathcal{S}_2$. For large positive (negative) values of U, entanglement is concentrated in the single- (zero-) spin sector. For $U = 0$ there is full entanglement in the charge sector and partial entanglement in each spin sector. The entanglement entropy is a parametric monotonic function of the sum of these partial concurrence measures.

entanglement overcomes in the noninteracting regime $U = 0$, reaching its maximum degree. However, there persists some degree of spin entanglement in both corresponding sectors. It is clear in Fig. 2 that the zero- and single-spin curves are interchanged with respect to the reversal of the Hubbard coupling from a repulsive to an attractive nature while the charge concurrence is an even function of U. For eigenstate $|\lambda_1\rangle$ the above picture is quite similar, only with $\mathcal{C}_0$ and $\mathcal{C}_1$ featuring inverted roles. It is interesting that the sum of all three partial concurrences gives the same value for both $|\lambda_1\rangle$ and $|\lambda_2\rangle$ states, as does the entanglement entropy [cf. Eq. (2)]. Even more remarkable is the fact that the total concurrence, $\mathcal{C}_c + \mathcal{C}_1 + \mathcal{C}_0$, is a monotonic function of the entanglement entropy. As such, the partial concurrences are able to provide a detailed description of the underlying quantum correlations and that can be applied to mixed (thermal) states as we are about to cover in the following section.

IV. PARTIAL CONCURRENCES AT FINITE TEMPERATURES

We now focus on the influence of temperature and magnetic field on the quantum entanglement of Hubbard dimers in equilibrium with a heat bath at temperature T. In this case, the system is in a mixed quantum state due to its weak coupling with the degrees of freedom of the heat reservoir. Therefore, the expectation values of the dimer correlations needed to evaluate the elements of ρ^X [Eq. (3)] as listed in Table II must incorporate both quantum and thermal averages. Within the canonical ensemble framework, given the expectation value
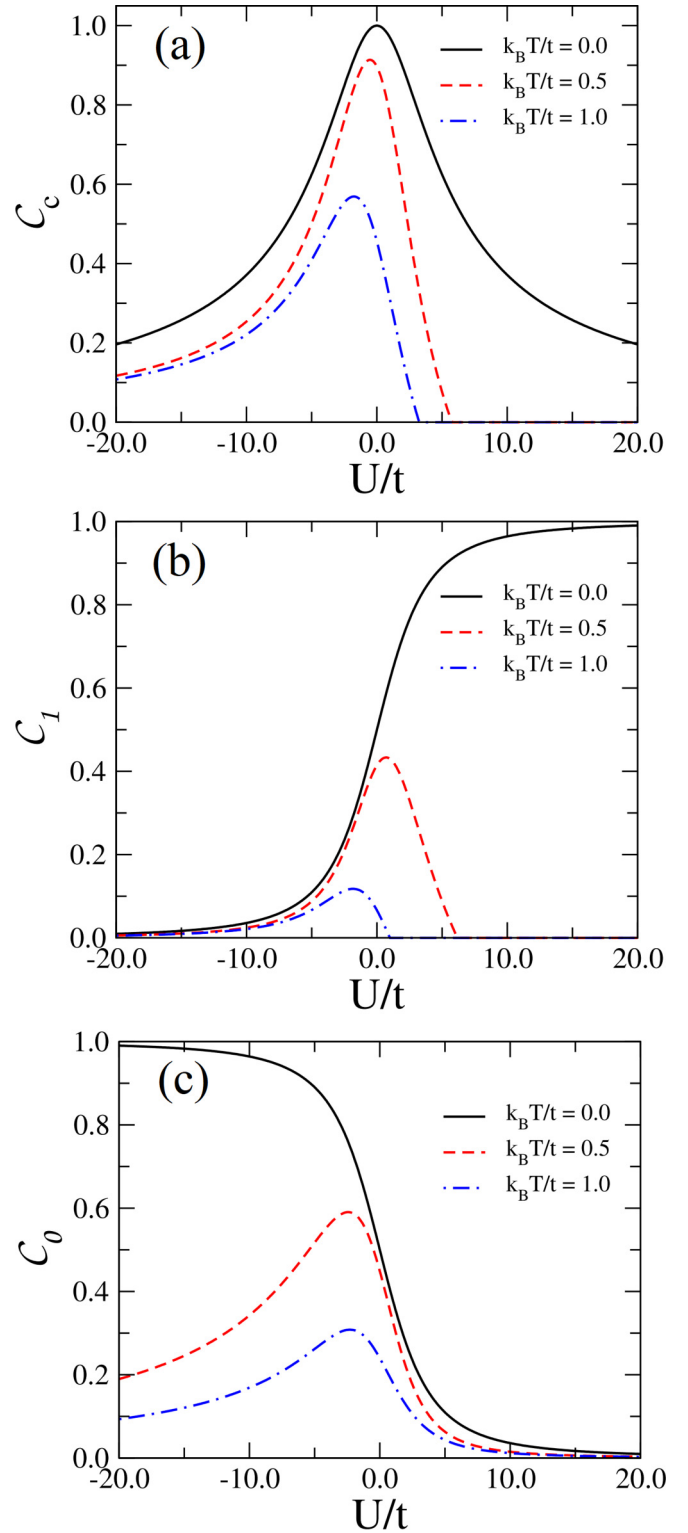
FIG. 3. (a) Charge $\mathcal{C}_c$, (b) single-spin $\mathcal{C}_1$, and (c) zero-spin $\mathcal{C}_0$ concurrences as a function of the Hubbard coupling U/t for some representative values of temperature at null magnetic field. The degrading effect of temperature is stronger for positive U. Charge and single-spin concurrences vanish above typical values of U that decrease as temperature is raised.

TABLE IV. Thermal averages of the relevant dimer correlations (density matrix elements) in each sector. The partition function $\mathcal{Z}$ is given by Eq. (4) and $\Delta = U^2 + 16t^2$.

Sector	$\langle u_+ \rangle_T$	$\langle u_- \rangle_T$	$\langle z \rangle_T$
Charge	$\frac{e^{-2\beta H}}{\mathcal{Z}}$	$\frac{e^{2\beta H}}{\mathcal{Z}}$	$[-4te^{\frac{-\beta U}{2}} \sinh(\frac{\beta\sqrt{\Delta}}{2})]/\mathcal{Z}\sqrt{\Delta}$
Single spin	$\frac{e^{2\beta H}}{\mathcal{Z}}$	$\frac{e^{-2\beta H}}{\mathcal{Z}}$	$\frac{e^{\frac{-\beta U}{2}}}{2\mathcal{Z}\Delta}[\Delta\cosh(\frac{\beta\sqrt{\Delta}}{2}) + U\sqrt{\Delta}\sinh(\frac{\beta\sqrt{\Delta}}{2})] - \frac{1}{2\mathcal{Z}}$
Zero spin	0	0	$\frac{e^{\frac{-\beta U}{2}}}{2\mathcal{Z}\Delta}[\Delta\cosh(\frac{\beta\sqrt{\Delta}}{2}) - U\sqrt{\Delta}\sinh(\frac{\beta\sqrt{\Delta}}{2})] - \frac{e^{-\beta U}}{2\mathcal{Z}}$

$\langle\mathcal{O}\rangle_i$ of a given quantum operator $\mathcal{O}$ in eigenstate $|\lambda_i\rangle$), its thermal average can be written as $\langle\mathcal{O}\rangle = (\sum_i \langle\mathcal{O}\rangle_i e^{-\lambda_i/k_B T})/\mathcal{Z}$, where $\mathcal{Z} = \sum_i e^{-\lambda_i/k_B T}$ is the partition function, here resulting in

$$\mathcal{Z} = 2e^{-\frac{\beta U}{2}} \cosh\left(\frac{\beta\sqrt{\Delta}}{2}\right) + e^{-\beta U} + 1 + 2\cosh(2\beta H). \quad (4)$$

Following the above prescription, we can obtain closed forms for the thermal averages of the relevant dimer correlations in each sector, as given in Table IV, from which the temperature dependence of the partial concurrences can be addressed.

We start off our analysis by plotting each partial concurrence as a function of the Hubbard coupling U for distinct temperatures in the absence of an external field, as reported in Fig. 3. For the charge sector, one notices that thermal fluctuations have a stronger degrading effect for large repulsive Hubbard couplings [Fig. 3(a)]. Actually, the charge quantum concurrence vanishes above a characteristic value of the Hubbard coupling that continuously decreases as temperature is raised. A similar trend occurs with concurrence in the single-spin sector [Fig. 3(b)], although it vanishes for a distinct Hubbard coupling value as compared with the charge concurrence at the same temperature. We get a rather different picture for the zero-spin partial concurrence [Fig. 3(c)]. In this case, although thermal fluctuations still act to spoil quantum correlations, the concurrence remains finite for any strength of the Hubbard interaction, vanishing only in the limit of $|U| \to \infty$ at finite temperatures. This feature is directly related to the fact that $\langle u_+ \rangle_T = \langle u_- \rangle_T = 0$ in this sector, so that the contribution to quantum entanglement comes exclusively from $\langle z \rangle_T$.

The explicit dependence of partial concurrences over temperature is shown in Fig. 4 for some representative values of the Hubbard coupling and $H/t = 1$. We recall that for negative U the ground state is $|\lambda_2\rangle$ which has maximum zero-spin concurrence, with residual single-spin and charge contributions. For positive U the ground state is the nonentangled saturated paramagnetic state. At $U = 0$ these states are degenerated. Thermal fluctuations reduce the degree of quantum entanglement in all sectors when the ground state features entanglement ($U \leqslant 0$). However, as discussed above, it vanishes at distinct threshold temperatures in the charge and single-spin sectors while it decreases continuously with rising temperatures as $1/T^2$ at the zero-spin sector. On the other hand, thermal fluctuations can *induce* some degree of quantum entanglement above the nonentangled ground state ($U > 0$). This is due to thermally induced mixing of excited entangled dimer states. However, this process is only effective

in the regime of low temperatures, for quantum entanglement is ultimately spoiled as the temperature is further increased.

The effect of the external magnetic field is reported in Fig. 5 for different temperatures. In all sectors, the magnetic field acts by reducing the degree of quantum entanglement. Here, we can also see that when the ground state is entangled, as it occurs for weak fields, thermal fluctuations deteriorate quantum correlation entanglement while thermally induced entanglement is developed at strong fields for which the ground state is nonentangled. The charge and single-spin concurrences vanish for any value of the magnetic field strength above the distinct characteristic temperatures.

Finally, we determine the threshold temperatures above which the concurrence in the charge and single-single spin sectors vanishes. These also depend on the Hubbard coupling, which splits the T-U parameter space into four regions, as depicted in Fig. 6. At low temperatures, quantum entanglement is distributed in all three sectors while at high temperatures there is some degree of quantum entanglement only in the zero-spin sector that fades away as $1/T^2$. However, the distinct values of the threshold temperature for which concurrence vanishes in the charge and single-spin sectors allows for the identification of two intermediate entanglement regimes. In one of them only the charge concurrence is zero while the single-spin concurrence vanishes in the other region. There is a specific value of the Hubbard coupling $U^*/t \simeq 5.53$ for which both concurrences vanish exactly at the same temperature. Therefore, charge entanglement is more robust against thermal fluctuations than single-spin entanglement for $U < U^*$, with reverse behavior taking place for $U > U^*$.

V. SUMMARY AND CONCLUSIONS

In summary, we have provided a detailed study of quantum entanglement in the half-filled Hubbard dimer in thermal equilibrium with a heat bath. An arbitrary dimer state belongs to a six-dimensional Hilbert space which restricts the use of standard entanglement measures. By mapping the local (site) modes into qubit state spaces, we were able to evaluate the effective concurrence in the charge, single-, and zero-spin sectors so as to discriminate how those degrees of freedom contribute to the overall entanglement. As a matter of fact, we found out that these partial concurrences can be added to provide a measure parametrically monotonic to the von Neumann entanglement entropy.

We went further to provide exact expressions for concurrence as a function of temperature, Hubbard coupling, and magnetic field strengths. At zero temperature and in the absence of magnetic field for strongly repulsive (attractive) Hubbard couplings, $U \to \infty$ ($U \to -\infty$), entanglement is
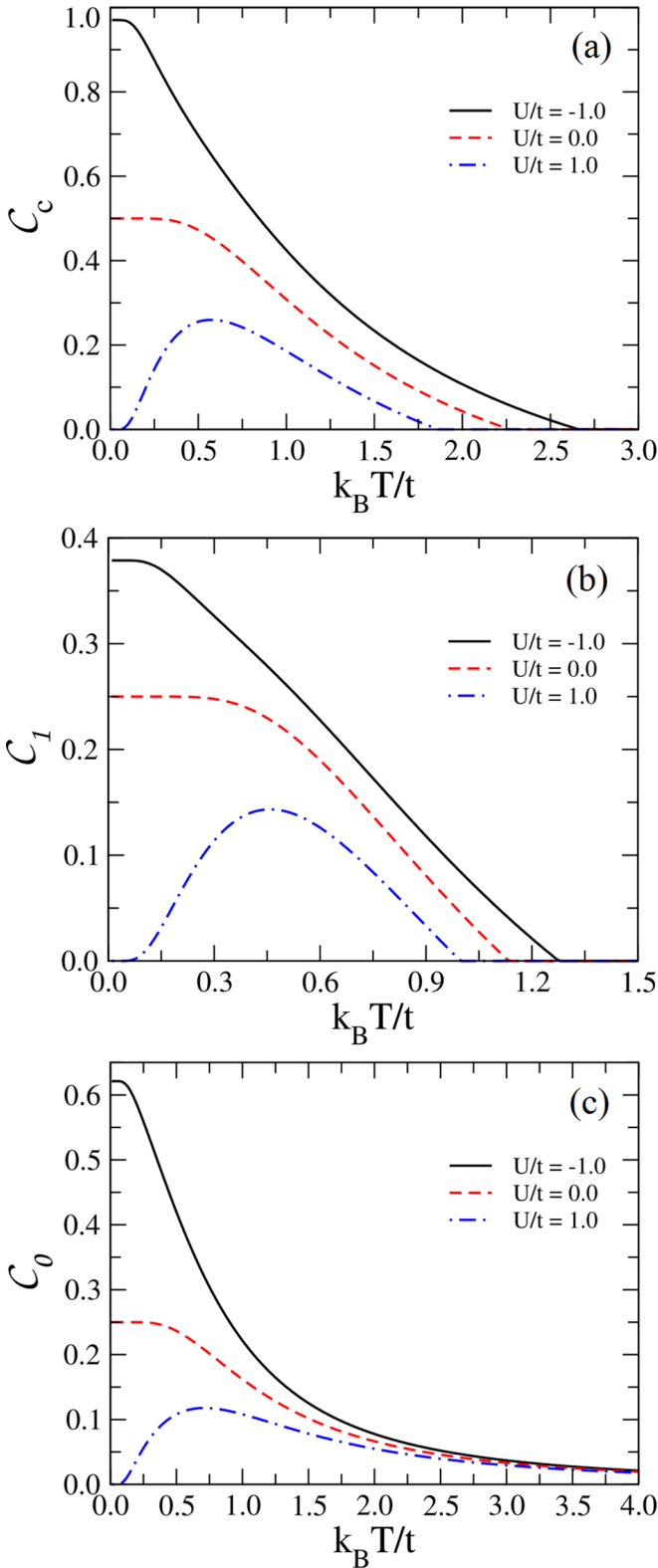
FIG. 4. (a) Charge $\mathcal{C}_c$, (b) single-spin $\mathcal{C}_1$, and (c) zero-spin $\mathcal{C}_0$ concurrences as a function of temperature for representative values of U/t and $H/t = 1$. For positive U, temperature leads to an overall degrading effect. For negative U, thermal fluctuations induce the emergence of some degree of quantum entanglement above the nonentangled ground state. Charge and single-spin concurrences strictly vanish above distinct threshold temperatures while the zero-spin concurrence continuously fades away as $1/T^2$.
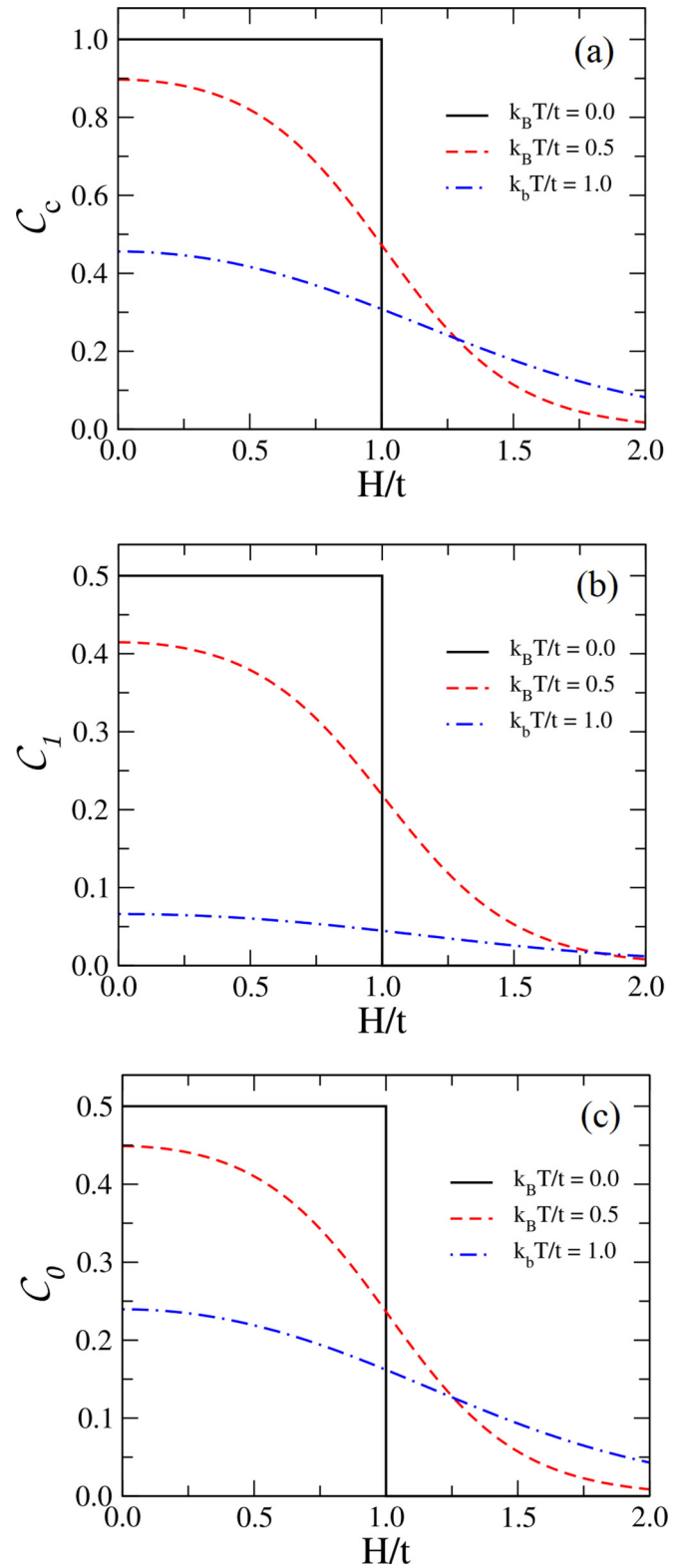
FIG. 5. (a) Charge $\mathcal{C}_c$, (b) single-spin $\mathcal{C}_1$, and (c) zero-spin $\mathcal{C}_0$ concurrences as a function of the magnetic field for some representative values of temperature and $U = 0$. Below the critical magnetic field $H/t = 1.0$, thermal fluctuations are harmful to entanglement. Above the critical field, some degree of quantum entanglement is thermally induced.
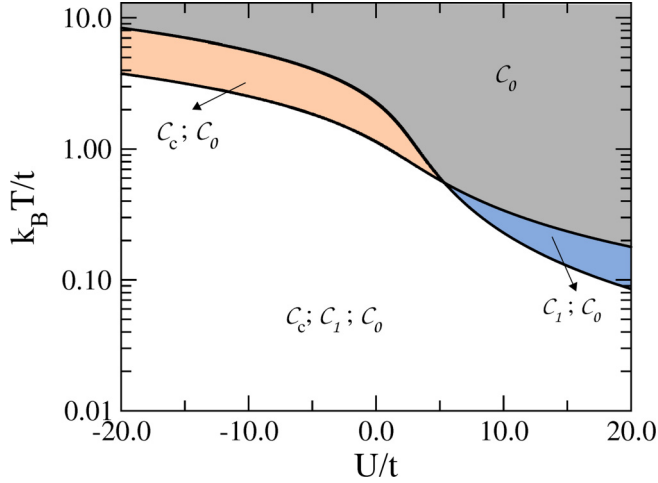
FIG. 6. Entanglement regimes in the temperature T vs Hubbard coupling U parameter space. At low finite temperatures, there is entanglement in all sectors. At high temperatures, entanglement persists only in the zero-spin sector, although it is proportional to $1/T^2$. There are also intermediate regions where entanglement in either charge or single-spin sectors persists while the other vanishes.

maximum and fully due to the zero-spin (single-spin) sector of degrees of freedom. In the noninteracting regime ($U = 0$) entanglement is maximum in the charge sector, featuring residual contributions from the zero- and single-spin sectors by the same amount.

We showed that thermal fluctuations have the expected damaging influence on quantum entanglement whenever the ground state is nonseparable. On the other hand, some degree of quantum concurrence can actually be induced by thermal fluctuations on a separable ground state due to the thermally induced occupation of excited entangled states. Quantum concurrences in the charge and single-spin sectors vanish above characteristic U-dependent temperatures while the zero-spin concurrence decays continuously as $1/T^2$ when temperature is raised. It is worth pointing out that spin chains usually present a threshold temperature for concurrence (see, e.g., Ref. [53]). On the other hand, concurrence was shown to decay continuously with temperature in a dimer model [54].

Putting it all together, we were able to address distinct regions in the $T \times U$ parameter space related to how quantum entanglement is distributed among the underlying degrees of freedom. The method used for evaluating the quantum concurrence in effective two-qubit sectors built out of local modes of itinerant electron systems [46,47,52] can be readily applied to larger Hubbard clusters and is not restricted to the half-filling condition. This is also particularly useful when one cannot have full access to the Hilbert space. Therefore, it proves to be a convenient tool to quantify quantum entanglement in other classes of strongly correlated many-body systems.

APPENDIX: OBTAINING ELEMENTS OF THE TWO-QUBIT SECTOR DENSITY MATRICES ρ^X

We show how to build the density matrices of Eq. (3) for each two-qubit sector in terms of the expectation values of fermionic operators as displayed in Table II. (This procedure can also be found in Ref. [51].) To begin with, we shall write down the density matrix associated with an arbitrary pure state $|\psi\rangle = \sum_i v_i |i\rangle$, with $\{|i\rangle\}$ being a complete basis set, as

$$\rho = \sum_{i,j} v_i v_j^* |i\rangle\langle j|. \tag{A1}$$

Each element of ρ thus reads $\rho_{i,j} \equiv \langle i|\rho|j\rangle = v_i v_j^*$. At this point we define projection operators $P_i|v_j\rangle = \delta_{i,j}|v_i\rangle$ so that $P_i|\psi\rangle = v_i|i\rangle$ ($P_i^2 = P_i$ as usual). We then write

$$\rho_{i,j} = \langle\psi|P_j T_{j,i} P_i|\psi\rangle, \tag{A2}$$

with $T_{j,i} \equiv |j\rangle\langle i| = T_{i,j}^\dagger$ being a transfer operator. Now it all comes down to expressing the projection and transfer operators in terms of fermionic annihilation and creation operators. The first step in this direction is to define the vacuum projector, above which everything else is generated [55],

$$|0;0\rangle\langle 0;0| = \mathcal{N}\left(\prod_\mu \exp(-c_\mu^\dagger c_\mu)\right), \tag{A3}$$

where $\mathcal{N}$ stands for normal ordering and μ specify the fermionic modes.

To illustrate how it works, let consider the charge sector first, spanned by $\{|1\rangle, |2\rangle, |3\rangle, |4\rangle\} \Leftrightarrow \{|0;0\rangle, |0;\uparrow\rangle, |\uparrow;0\rangle, |\uparrow;\uparrow\rangle\}$. The projection operators are given by

$$P_1 \Leftrightarrow |0;0\rangle\langle 0;0|, \tag{A4}$$

$$P_2 \Leftrightarrow c_{2\uparrow}^\dagger|0;0\rangle\langle 0;0|c_{2\uparrow}, \tag{A5}$$

$$P_3 \Leftrightarrow c_{1\uparrow}^\dagger|0;0\rangle\langle 0;0|c_{1\uparrow}, \tag{A6}$$

$$P_4 \Leftrightarrow c_{1\uparrow}^\dagger c_{2\uparrow}^\dagger|0;0\rangle\langle 0;0|c_{2\uparrow}c_{1\uparrow}. \tag{A7}$$

In this case, note that there are only two modes involved, namely $\mu = c_{1\uparrow}, c_{2\uparrow}$. By expanding the vacuum projector accordingly [see Eq. (A3)], we end up with

$$\mathbf{P}^C = \{(1 - n_{1\uparrow})(1 - n_{2\uparrow}), (1 - n_{1\uparrow})n_{2\uparrow}, n_{1\uparrow}(1 - n_{2\uparrow}),$$
$$n_{1\uparrow}n_{2\uparrow}\}, \tag{A8}$$

where it is straightforward to spot that $\sum_i P_i = 1$ (completeness).

Due to total spin and charge conservation (cf. Table I), the only off-diagonal terms in Eq. (3) different from zero are $z^X \equiv \rho_{2,3}$ and $(z^X)^*$. Then we only need to evaluate one transition operator, namely

$$T_{3,2} \Leftrightarrow c_{1\uparrow}^\dagger|0;0\rangle\langle 0;0|c_{2\uparrow}. \tag{A9}$$

In general those can be written in the form $T_{i,j} = P_i \tilde{T}_{i,j}$. For the charge sector, $\tilde{T}_{3,2} = c_{1\uparrow}^\dagger c_{2\uparrow}$. We are now ready to build ρ^C by plugging the expressions we have just worked out into Eq. (A2), thereby obtaining the elements listed in Table II.

Note that as the modes $\mu = 1 \downarrow, 2 \downarrow$ were ruled out when expanding the vacuum projector in Eq. (A3), the resulting set of projection operators was complete, entailing a normalized density matrix in the charge sector. Now, for the two remaining sectors, $\{|\uparrow;\uparrow\rangle, |\uparrow;\downarrow\rangle, |\downarrow;\uparrow\rangle, |\downarrow;\downarrow\rangle\}$ (single spin; $X = 1$) and $\{|0;0\rangle, |0;\uparrow\downarrow\rangle, |\uparrow\downarrow;0\rangle, |\uparrow;\uparrow\downarrow\rangle\}$ (zero spin; $X = 0$), the vacuum projector must take all four fermionic modes into account. Following the same procedure as above, we obtain

$$\mathbf{P}^1 = \{n_{1\uparrow}(1 - n_{1\downarrow})n_{2\uparrow}(1 - n_{2\downarrow}), n_{1\uparrow}(1 - n_{1\downarrow})(1 - n_{2\uparrow})n_{2\downarrow},$$

$$(1 - n_{1\uparrow})n_{1\downarrow}n_{2\uparrow}(1 - n_{2\downarrow}), (1 - n_{1\uparrow})n_{1\downarrow}(1 - n_{2\uparrow})n_{2\downarrow}\},$$

$$\text{(A10)}$$

$$\mathbf{P}^0 = \{(1 - n_{1\uparrow})(1 - n_{1\downarrow})(1 - n_{2\uparrow})(1 - n_{2\downarrow}),$$

$$(1 - n_{1\uparrow})(1 - n_{1\downarrow})n_{2\uparrow}n_{2\downarrow},$$

$$n_{1\uparrow}n_{1\downarrow}(1 - n_{2\uparrow})(1 - n_{2\downarrow}), n_{1\uparrow}n_{1\downarrow}n_{2\uparrow}n_{2\downarrow}\}. \quad \text{(A11)}$$

The transfer operators $T_{3,2} = P_3 \tilde{T}_{3,2}$ are such that

$$\tilde{T}_{3,2} = c_{2\uparrow}^\dagger c_{2\downarrow} c_{1\downarrow}^\dagger c_{1\uparrow} \quad \text{(for } X = 1\text{)}, \quad \text{(A12)}$$

$$\tilde{T}_{3,2} = c_{1\uparrow}^\dagger c_{1\downarrow}^\dagger c_{2\downarrow} c_{2\uparrow} \quad \text{(for } X = 0\text{)}. \quad \text{(A13)}$$

And once again, we substitute everything back into Eq. (A2) to complete Table II.

The resulting density matrices for those two sectors are no longer normalized as one may have guessed by examining $\mathbf{P}^1$ and $\mathbf{P}^0$. Although each set is *effectively* complete when only the states belonging to the corresponding sector are involved, it is not when the expectation values are taken in the states listed in Table I, for example. This is so because ρ^1 and ρ^0 are *projections* of the full density matrix with 16×16 entries. Still, that does not prevent us from evaluating the correlations within the density matrices and, as a matter of fact, they do account for genuine partial entanglement as they can be added with the charge-sector concurrence to provide us with a measure that behaves monotonically with the von Neumann entanglement entropy.

[1] R. Horodecki, P. Horodecki, M. Horodecki, and K. Horodecki, Rev. Mod. Phys. **81**, 865 (2009).

[2] L. Amico, R. Fazio, A. Osterloh, and V. Vedral, Rev. Mod. Phys. **80**, 517 (2008).

[3] G. De Chiara and A. Sanpera, Rep. Prog. Phys. **81**, 074002 (2018).

[4] M. B. Plenio and S. Virmani, Quantum Inf. Comput. **7**, 1 (2007).

[5] N. Laflorencie, Phys. Rep. **646**, 1 (2016).

[6] D. J. Luitz, N. Laflorencie, and F. Alet, J. Stat. Mech. (2014) P08007.

[7] F. Parisen Toldin and F. F. Assaad, Phys. Rev. Lett. **121**, 200602 (2018).

[8] W. Zhu, Z. Huang, and Y.-C. He, Phys. Rev. B **99**, 235109 (2019).

[9] M. C. Arnesen, S. Bose, and V. Vedral, Phys. Rev. Lett. **87**, 017901 (2001).

[10] T. Werlang, G. A. P. Ribeiro, and G. Rigolin, Int. J. Mod. Phys. B **27**, 1345032 (2013).

[11] C. H. Bennett, D. P. DiVincenzo, J. A. Smolin, and W. K. Wootters, Phys. Rev. A **54**, 3824 (1996).

[12] W. K. Wootters, Phys. Rev. Lett. **80**, 2245 (1998).

[13] W. K. Wootters, Quantum Inf. Comput. **1**, 27 (2001).

[14] N. Killoran, M. Cramer, and M. B. Plenio, Phys. Rev. Lett. **112**, 150501 (2014).

[15] R. Lo Franco and G. Compagno, Phys. Rev. Lett. **120**, 240403 (2018).

[16] J. Schliemann, D. Loss, and A. H. MacDonald, Phys. Rev. B **63**, 085311 (2001).

[17] J. Schliemann, J. I. Cirac, M. Kuś, M. Lewenstein, and D. Loss, Phys. Rev. A **64**, 022303 (2001).

[18] R. Paškauskas and L. You, Phys. Rev. A **64**, 042310 (2001).

[19] Y. S. Li, B. Zeng, X. S. Liu, and G. L. Long, Phys. Rev. A **64**, 054302 (2001).

[20] K. Eckert, J. Schliemann, D. Bruß, and M. Lewenstein, Ann. Phys **299**, 88 (2002).

[21] P. Zanardi, Phys. Rev. A **65**, 042101 (2002).

[22] P. Zanardi and X. Wang, J. Phys. A: Math. Gen. **35**, 7947 (2002).

[23] J. R. Gittings and A. J. Fisher, Phys. Rev. A **66**, 032305 (2002).

[24] H. M. Wiseman and J. A. Vaccaro, Phys. Rev. Lett. **91**, 097902 (2003).

[25] Y. Shi, Phys. Rev. A **67**, 024301 (2003).

[26] G. C. Ghirardi and L. Marinatto, Phys. Rev. A **70**, 012109 (2004).

[27] M. R. Dowling, A. C. Doherty, and H. M. Wiseman, Phys. Rev. A **73**, 052323 (2006).

[28] A. Ramšak, I. Sega, and J. H. Jefferson, Phys. Rev. A **74**, 010304(R) (2006).

[29] F. Buscemi, P. Bordone, and A. Bertoni, Phys. Rev. A **75**, 032301 (2007).

[30] A. P. Balachandran, T. R. Govindarajan, A. R. de Queiroz, and A. F. Reyes-Lega, Phys. Rev. Lett. **110**, 080503 (2013).

[31] N. Friis, A. R. Lee, and D. E. Bruschi, Phys. Rev. A **87**, 022338 (2013).

[32] B. J. Dalton, L. Heaney, J. Goold, B. M. Garraway, and T. Busch, New J. Phys. **16**, 013026 (2014).

[33] N. Gigena and R. Rossignoli, Phys. Rev. A **92**, 042326 (2015).

[34] R. L. Franco and G. Compagno, Sci. Rep. **6**, 20603 (2016).

[35] M. Johansson, Phys. Rev. A **93**, 022328 (2016).

[36] M. Johansson and Z. Raissi, Phys. Rev. A **94**, 042319 (2016).

[37] N. Gigena and R. Rossignoli, Phys. Rev. A **95**, 062320 (2017).

[38] A. C. Lourenço, T. Debarba, and E. I. Duzzioni, Phys. Rev. A **99**, 012341 (2019).

[39] S. Chin and J. Huh, Phys. Rev. A **99**, 052345 (2019).

[40] T. Grover, Phys. Rev. Lett. **111**, 130402 (2013).

[41] A. Anfossi, P. Giorda, A. Montorsi, and F. Traversa, Phys. Rev. Lett. **95**, 056402 (2005).

[42] D. Larsson and H. Johannesson, Phys. Rev. Lett. **95**, 196406 (2005).

[43] O. S. Zozulya, M. Haque, and K. Schoutens, Phys. Rev. A **78**, 042326 (2008).

[44] L. Zhu, C. Duan, and W. Wang, J. Magn. Magn. Mater. **321**, 56 (2009).

[45] A. N. Ribeiro and C. A. Macedo, Phys. Rev. A **86**, 022320 (2012).

[46] S. J. Gu, S. S. Deng, Y. Q. Li, and H. Q. Lin, Phys. Rev. Lett. **93**, 086402 (2004).

[47] S. S. Deng and S. J. Gu, Chin. Phys. Lett. **22**, 804 (2005).

[48] M. Nalbandyan, H. Lazaryan, O. Rojas, S. M. de Souza, and N. Ananikian, J. Phys. Soc. Jpn. **83**, 074001 (2014).

[49] T. Fukuhara, S. Hild, J. Zeiher, P. Schauß, I. Bloch, M. Endres, and C. Gross, Phys. Rev. Lett. **115**, 035302 (2015).

[50] J. Torrico, M. Rojas, M. S. S. Pereira, J. Strecka, and M. L. Lyra, Phys. Rev. B **93**, 014428 (2016).

[51] A. Rycerz, New. J. Phys. **19**, 053025 (2017).

[52] H. S. Sousa, M. S. S. Pereira, I. N. de Oliveira, J. Strecka, and M. L. Lyra, Phys. Rev. E **97**, 052115 (2018).

[53] I. Bose and A. Tribedi, Phys. Rev. A **72**, 022314 (2005).

[54] J.-Q. Liao, J.-F. Huang, L.-M. Kuang, and C. P. Sun, Phys. Rev. A **82**, 052109 (2010).

[55] B. J. Dalton, J. Jeffers, and S. M. Barnett, *Phase Space Methods for Degenerate Quantum Gases*, 1st ed. (Oxford University Press, Oxford, UK, 2014).